



Infrared Absorption and Its Sources of CdZnTe at Cryogenic Temperature

Hiroshi Maeshima^{1,2} · Kosei Matsumoto^{1,2} · Yasuhiro Hirahara³ · Takao Nakagawa² · Ryoichi Koga³ · Yusuke Hanamura³ · Takehiko Wada² · Koichi Nagase² · Shinki Oyabu⁴ · Toyoaki Suzuki² · Takuma Kokusho⁵ · Hidehiro Kaneda⁵ · Daichi Ishikawa⁵

Received: 2 September 2021 / Accepted: 17 November 2021 / Published online: 3 January 2022
© The Author(s) 2021

Abstract

To reveal the causes of infrared absorption in the wavelength region between electronic and lattice absorptions, we measured the temperature dependence of the absorption coefficient of *p*-type low-resistivity ($\sim 10^2 \Omega\text{cm}$) CdZnTe crystals. We measured the absorption coefficients of CdZnTe crystals in four wavelength bands ($\lambda = 6.45, 10.6, 11.6, 15.1 \mu\text{m}$) over the temperature range of $T = 8.6\text{--}300 \text{ K}$ with an originally developed system. The CdZnTe absorption coefficient was measured to be $\alpha = 0.3\text{--}0.5 \text{ cm}^{-1}$ at $T = 300 \text{ K}$ and $\alpha = 0.4\text{--}0.9 \text{ cm}^{-1}$ at $T = 8.6 \text{ K}$ in the investigated wavelength range. With an absorption model based on transitions of free holes and holes trapped at an acceptor level, we conclude that the absorption due to free holes at $T = 150\text{--}300 \text{ K}$ and that due to trapped-holes at $T < 50 \text{ K}$ are dominant absorption causes in CdZnTe. We also discuss a method to predict the CdZnTe absorption coefficient at cryogenic temperature based on the room-temperature resistivity.

Keywords CdZnTe · infrared transmittance · cryogenic material · absorption coefficient

Introduction

Cadmium zinc telluride (CdZnTe) is a type II-VI compound semiconductor, commonly used as an X-ray detector¹ or substrate for the growth of epitaxial layers of mercury cadmium telluride (MCT) for infrared detector arrays.² Large-size single-crystal CdZnTe growth techniques have been developed for such applications. Single-crystal ingots of CdZnTe with 5-inch diameter are now commercially available, with 6-inch crystals in the experimental stage.³

CdZnTe is also promising as an infrared optical material with wavelengths between 5–20 μm . In general, the electronic and lattice absorptions characterize intrinsic absorption, which is the immutable absorption even for pure semiconductors.⁴ CdZnTe has little intrinsic absorption in the infrared wavelength range. Also, CdZnTe has extrinsic absorption, such as free-carrier absorption due to impurities and attenuation due to Te precipitates.^{3,5} As a result, we anticipate that CdZnTe can be used as an infrared optical material by controlling its extrinsic properties (e.g., impurity or Te precipitates).

In addition, these infrared materials are frequently used in low-temperature environments to reduce thermal background radiation, particularly in astronomical observation

✉ Hiroshi Maeshima
maeshima@ir.isas.jaxa.jp

Takao Nakagawa
nakagawa@ir.isas.jaxa.jp

Ryoichi Koga
koga.ryoichi.y9@a.mail.nagoyau.ac.jp

¹ Graduate School of Science, The University of Tokyo, 7-3-1 Hongo, Bunkyo-ku, Tokyo 113-0033, Japan

² Institute of Space and Astronautical Science, Japan Aerospace Exploration Agency, 3-1-1 Yoshinodai, Chuo-ku, Sagami-hara, Kanagawa 252-5210, Japan

³ Graduate School of Environmental Studies, Nagoya University, Furo-cho, Chikusa-ku, Nagoya, Aichi 464-8601, Japan

⁴ Institute of Liberal Arts and Sciences, Tokushima University, 1-1 Minami-Jyosanjima, Tokushima-shi, Tokushima 770-8502, Japan

⁵ Graduate School of Science, Nagoya University, Furo-cho, Chikusa-ku, Nagoya, Aichi 464-8602, Japan

Table 1 Properties of the CdZnTe single crystals. The specifications are measured at room temperature. (*Ra*: arithmetic average roughness of the surface)

Sample	Incident-surface size [mm ²]	Thickness [mm]	Resistivity [Ωcm]	Conductivity type	Te particle size [μm]	<i>Ra</i> [nm]
lowR-t1	7 × 7	1.01	(0.5-1.3) × 10 ²	<i>p</i>	< 2	< 1
lowR-t10	7 × 7	9.91	(0.5-1.3) × 10 ²	<i>p</i>	< 2	< 1

optics (e.g., SPICA Mid-Infrared Instrument⁶ on board the SPICA mission¹).^{7,8} As a result, the ability of infrared materials to transmit light at low temperatures is essential for astronomical applications.

An immersion grating is an optical material application of CdZnTe.⁹ Immersion gratings are diffraction gratings with a grooved surface immersed in a material with high refractive index.^{10,11} CdZnTe is an attractive material for immersion grating at wavelengths of $\lambda = 10\text{--}20\ \mu\text{m}$ due to its high refractive index ($n \sim 2.7$) and transparency.^{12,13} Owing to its high refractive index n , an immersion grating can be downsized $1/n$ in length compared to conventional gratings. In size-constrained situations, the $1/n$ -downsizing of a grating has a significant impact on the design of a compact optical system (e.g., astronomical satellites, systems in cryostat dewars). CdZnTe-immersion grating is expected to be applied in space telescopes.¹⁴

The room-temperature absorption coefficient in infrared wavelengths is known to be resistivity-dependent. Kaji et al.¹³ investigated the absorption coefficient of CdZnTe crystals with resistivities of $\rho = 3.5 \times 10^{10}\ \Omega\text{cm}$ and $\rho \sim 1 \times 10^2\ \Omega\text{cm}$ at room temperature. They discovered that the absorption coefficient of low-resistivity CdZnTe was higher than that of high-resistivity CdZnTe and increased with wavelength at $\lambda = 5\text{--}20\ \mu\text{m}$. This high absorption is considered to be caused by free-carrier absorption.^{4,13} When low-resistivity CdZnTe is cooled down to cryogenic temperature, the free-carrier absorption coefficient becomes smaller than the coefficient at room temperature due to free-carrier freeze-out. Therefore, low-resistivity CdZnTe, which is more readily available than high-resistivity CdZnTe, is expected to be suitable for cryogenic infrared materials. However, because there are few previous studies on the optical performance of CdZnTe at low temperatures, absorption causes in CdZnTe at cryogenic temperature are unknown. The optical performance of low-resistivity CdZnTe must be studied in order to develop cryogenic infrared materials (e.g., immersion gratings).⁹

In this paper, we investigate the process for mid-infrared photon absorption by measuring the temperature dependence of the absorption coefficient of CdZnTe in the temperature

range of $T = 8.6\text{--}300\ \text{K}$. We expect cryogenic absorption coefficients of CdZnTe crystals to be predictable from room-temperature physical properties after revealing the possible processes for the mid-infrared photon absorption.

Method

This section describes the method used to measure the absorption coefficient. First, we describe the derivation method of the absorption coefficient from transmittance measurements. Taking into account the multiple reflections, we express the total transmittance τ as follows:

$$\tau = \frac{(1 - R)^2 \exp(-\alpha t)}{1 - R^2 \exp(-2\alpha t)}, \quad (1)$$

where α is the absorption coefficient, $R = (n - 1)^2 / (n + 1)^2$ is the Fresnel surface reflectivity, and t is the sample thickness.⁵ We can estimate the absorption coefficient by measuring the transmittance (τ_1, τ_2) of samples made of the same material but with different thicknesses (t_1, t_2) as follows:

$$\alpha = -\frac{\ln(\tau_1/\tau_2)}{t_1 - t_2} + X, \quad (2)$$

$$X = \frac{1}{t_1 - t_2} \ln \left[\frac{1 - R^2 \exp(-2\alpha t_2)}{1 - R^2 \exp(-2\alpha t_1)} \right]. \quad (3)$$

In this case, we assume the common surface reflectivity R . The term X arises from the effect of the multiple reflections. In the case of the refractive index $n = 2.7$, X/α is less than 0.1 at any α value. If X is included in the systematic error, α can be approximated as follows:

$$\alpha = -\frac{\ln(\tau_1/\tau_2)}{t_1 - t_2}. \quad (4)$$

Therefore, α can be estimated without assuming the R value. In this study, we use Eq. 4 to calculate α from the measured transmittance τ .

Table 1 shows the specifications of the CdZnTe samples used in this study. JX Nippon Mining & Metals Corporation produced the Cd_{0.96}Zn_{0.04}Te single crystals used in the measurements. The vertical gradient freezing (VGF) method is used to make the CdZnTe ingot. In the main text, the

¹ SPICA had been a candidate for the fifth M-class mission in the ESA Cosmic Vision but was canceled on financial grounds in October 2020.

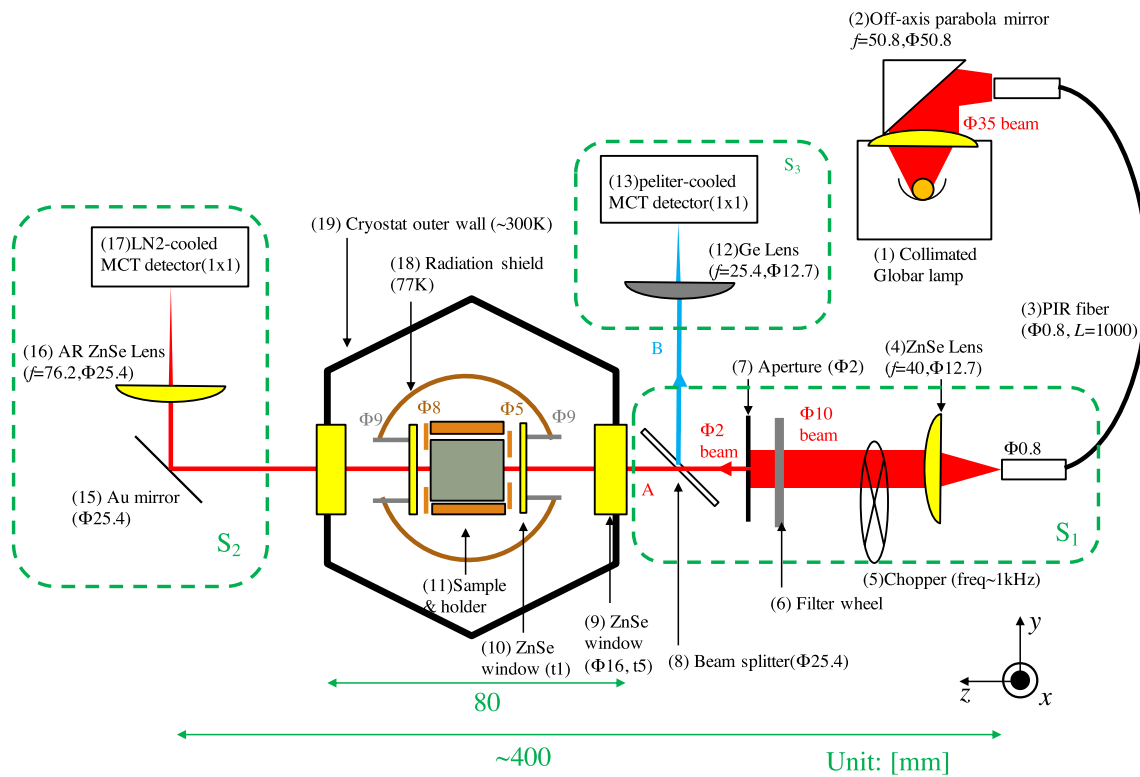


Fig. 1 The measurement system. Each component is described in the text. Red and blue lines show the beam path. Dimensions are in millimeters. Focal length f is indicated for each lens. Thickness, diameter, length of each component are denoted by t , Φ , and L , respectively. Components in green dashed areas are mounted on each stage plate.

The stages S_1 , S_2 , S_3 can move in two directions vertical to the beam axis. The temperatures of the cryostat outer wall (19) and the radiation shield (18) are ~ 300 K and ~ 77 K, respectively, when a sample is cooled to the lowest temperature (8.6 K). Details of sample holder structure are described in Appendix B (Color figure online).

Table II Specifications of the measurement system

Parameters	Specifications	Notes
Light source	Silicon Nitride Globar	
Detectors	MCT detectors	LN ₂ -cooled/Peltier-cooled
Beam size	$\phi 2$ mm	
Temperature	$T = 8.6$ -300 K	see results section
Incident angle	$\sim 0^\circ$	
Band center \pm HWHM	$\lambda = 6.45 \pm 0.05, 10.6 \pm 0.8, 11.6 \pm 0.4, 15.1 \pm 0.6 \mu\text{m}$	

conductivity is controlled to p -type for the ingot and n -type for Appendix A. The substrates were then cut from the ingot. To confirm whether the predicted change in absorption coefficient with temperature exists, we controlled the resistivity to the same order ($\rho \sim 10^2 \Omega\text{cm}$) as the low-resistivity CdZnTe measured by Sarugaku et al.⁵ The ingot was then annealed to reduce scattering caused by Te precipitates by reducing precipitate size.³ The incident and exit surfaces are polished with a surface roughness of $Ra < 1$ nm to reduce scattering loss on the surface, where Ra is the calculated average roughness. To derive the absorption coefficient from the thickness dependence of the transmittance, samples with

two types of thicknesses, lowR-t1 and lowR-t10, are taken from the same ingot.

Generally, infrared transmittance is measured using a Fourier transform spectrometer (FTS). However, commercial FTS products have numerous constraints, making it practically difficult to adjust the position of the sample cooling stage. In addition, for thick substrates with a high refractive index (n) such as CdZnTe, transmittance measurement with a typical uncollimated FTS may result in significant systematic uncertainty due to the defocus effect.¹³ Installing a thick and high- n substrate in the sample compartment lengthens the optical path and shifts the

detector's focus position backward. Furthermore, the focal position is wavelength-dependent due to the wavelength dependence of the refractive index n . Because of this, large systematic defocus errors in transmittance measurement occur.

We built an original measurement system on an optical bench using a collimated beam and a cryostat to solve the adjustment difficulty and the defocus problem. We anticipated that the defocus effect would not be an issue by irradiating the collimated beam with the sample.¹³ Figure 1 shows the originally developed measurement system and Table II summarizes the system's specifications. To irradiate samples, we use a Globar lamp (1 in Fig. 1; SLS303, Thorlabs Japan Inc.) as an infrared light source. The lamp's light beam is guided by a polycrystalline infrared fiber (3) and is recollimated with a lens (4). We can change the wavelength of the collimated beam by mounting four bandpass filters ($\lambda = 6.45, 10.6, 11.6, 15.1 \mu\text{m}$; listed in Table II) in the filter wheel. To pass through the sample-holder aperture ($\phi 5 \text{ mm}$), the infrared light beam is adjusted to $\phi 2 \text{ mm}$ with an aperture (7). To monitor the time variation, we split the incident beam with a beam splitter (8), and the reflected beam B is focused on a Pelier-cooled MCT detector (13; PVM1-4TE-10.6-1x1-TO8-wZnSeAR-35; VIGO System S.A.). Beam A is transmitted to the sample (11) with an incident angle of $\sim 0^\circ$ and focused on another liquid-nitrogen (LN_2) cooled MCT detector (17: IOH-1064, Bomem Inc.) to measure the transmitted light power. We use an optical chopper (5; model 300 CD, Scitec Instruments) with a frequency of $\sim 1 \text{ kHz}$ and lock-in amplifiers (SR830, Standard Research Systems) connected to the detectors because the incident beam to the sample is relatively faint ($\sim 10^{-5} \text{ W cm}^{-2}$ in the $10.6 \mu\text{m}$ band right after the aperture 7).

We used a cryostat with a two-stage Gifford-McMahon cryocooler (PS24SS; Nagase & Co., Ltd) to cool a sample to cryogenic temperature. Furthermore, we attached anti-reflective-coated (AR-coated) ZnSe windows with thicknesses of 5 mm and 1 mm to the vacuum chamber and the radiation shield in the chamber, respectively, to transmit the mid-infrared beam. To avoid thermal conduction, we reduced the gas pressure inside the chamber to $< 10^{-2} \text{ Pa}$. A built-in calibrated Si-diode sensor measures the temperature of the cold head. To stabilize the temperature during measurement, we installed a heater near the cold head. We prepared two types of holders to cool samples: one for the thick sample and the other for the thin sample. The details of the holders are described in Appendix B.

Next, we described the measurement procedure. A sample's transmittance τ is calculated as

$$\tau(\lambda, T) = \frac{V_{A,\text{smp}}(\lambda, T)/V_{B,\text{smp}}(\lambda, T)}{V_{A,\text{ref}}(\lambda)/V_{B,\text{ref}}(\lambda)}, \quad (5)$$

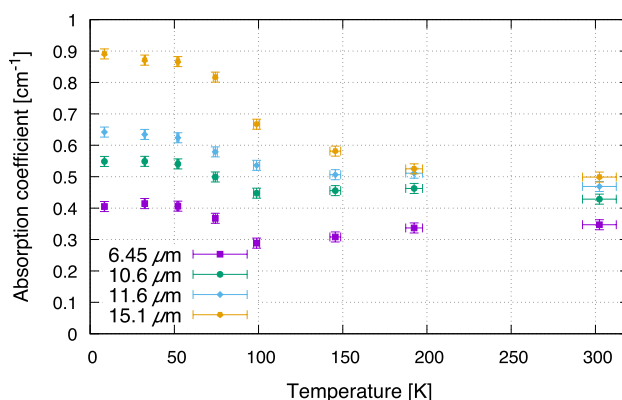


Fig. 2 Absorption coefficient of CdZnTe at a wavelength of $\lambda = 6.45$ (purple), 10.6 (green), 11.6 (sky blue), and $15.1 \mu\text{m}$ (orange) μm . Vertical error bars show the 1σ uncertainty range of the absorption coefficient. Horizontal error bars show the accuracy of the temperature (Color figure online).

where $V_{x,\text{smp}}$ ($x = A$ or B) is the power detected on the detector of the x side of the beam with the sample and $V_{x,\text{ref}}$ is the power detected without the sample. To reduce the effect of time variation in incident light powers, we measured powers $V_{A,\text{smp}}$ and $V_{B,\text{smp}}$ simultaneously, as well as $V_{A,\text{ref}}$ and $V_{B,\text{ref}}$. We measured the $V_{A,\text{ref}}(\lambda)/V_{B,\text{ref}}(\lambda)$ at 300 K because the denominator $V_{A,\text{ref}}/V_{B,\text{ref}}$ is a constant value against temperature change. We measured the transmittance of two samples at the four bands described in Table II.

We cooled the samples at a rate of $< 6 \text{ K min}^{-1}$ to reduce thermal stress on the sample. During the transmittance measurement, the temperature of the cold head is controlled within $\pm 0.1 \text{ K}$ by using a heater controller. Because thermal shrinkage affects the beam vignetting, it is necessary to optimize the beam alignment during the measurement. Also, because the sample's position shifts by $\sim 1 \text{ mm}$ due to thermal shrinkage of the cold-head shaft, the beam power measured at the aperture may be vignetted at $\sim 3\%$. Thus, at each measurement temperature, we adjusted the stages S_1 , S_2 , and S_3 (see Fig. 1) in two vertical directions to the optical axis to allow the beam to pass through the center of the holder aperture. Subsequently, because the beam is collimated, the adjustment does not affect the focal length. As a result, we can adjust the beam position by adjusting the three stages. We measure the transmittance of thin and thick samples at various temperatures ranging from about $T = 300 \text{ K}$ to the lowest temperature (8.6 K ; see the following section).

Results

Figure 2 shows the absorption coefficients α of CdZnTe at $\lambda = 6.45, 10.6, 11.6,$ and $15.1 \mu\text{m}$ from room temperature to a cryogenic temperature at $T = 8.6 \text{ K}$.

We calibrate the systematic temperature error caused by the Seebeck effect by averaging the measured temperatures with the voltage polarity swapped. Based on the measurement system's specification accuracy (Model 218, Lakeshore Inc.), we estimate the temperature uncertainty as $\Delta T = 10, 5, 2, 1, 0.3, 0.05$ K at $T \sim 300, 200, 100, 50, 8.6$ K, respectively.

The uncertainty of the measured absorption coefficient is mainly caused by the reproducibility of optimizing the beam alignment described in the previous section. We thus assume that the reproducibility is the same for all cases of temperatures, wavelengths bands, and samples because we perform the stage adjustments following a similar approach. We measure the 1σ reproducibility of the transmittance $\Delta\tau/\tau = 0.011$ at 300 K and apply it to all the measured τ . From the error propagation law using Eq. 4, the 1σ uncertainty of α is estimated as $\Delta\alpha = 0.016 \text{ cm}^{-1}$.

As shown in Fig. 2, the measured α ranges from 0.3–0.5 cm^{-1} at $T = 300$ K and from 0.4–0.9 cm^{-1} at $T = 8.6$ K. At each temperature, the absorption coefficient α at the longer wavelength is larger than the value at the shorter wavelength. At $T = 100$ –300 K, the $\alpha(\lambda = 6.45 \mu\text{m})$ decreases with cooling, whereas the $\alpha(\lambda = 15.1 \mu\text{m})$ increases. In the temperature range of $T = 100$ –300 K, the temperature dependencies of $\alpha(\lambda = 10.6 \mu\text{m})$ and $\alpha(\lambda = 11.6 \mu\text{m})$ are small compared to the uncertainty. At all measured wavelengths, the absorption coefficient α increases by 16–40% from $T = 100$ K to $T = 50$ K. At $T < 50$ K, the temperature dependence of the α becomes small. The dependence of the absorption coefficients on temperature is discussed in the next section.

The result is then compared to the free-carrier expectation.⁵ The absorption rate caused by free carriers is proportional to the free carrier's density. At low temperatures, the carrier density is proportional to $f(T) = \exp(-E_a/2k_B T)$, where E_a is the energy separation of the donor or acceptor level from the conduction or valence band¹⁵ and k_B is the Boltzmann constant. If we assume that E_a of CdZnTe is consistent with that of CdTe ($E_a = 60 \text{ meV}$)¹⁶ for simplicity, cooling from $T = 300$ K to $T < 50$ K reduces the free-carrier density by less than $f(T = 50 \text{ K})/f(T = 300 \text{ K}) \sim 0.003$. The proportional relationship would also reduce the free-carrier absorption coefficient by less than ~ 0.003 times. Even for the case of multi-impurity levels, free-carriers are estimated to be frozen out because the reported acceptor levels of CdTe are $\sim 60 \text{ meV}$ or $\sim 150 \text{ meV}$.^{16,21} In contrast to the free-carrier expectation, the measured α increases by about 1.3–1.8 times from $T = 300$ K to $T = 8.6$ K.⁵ In the following section, we discuss this apparent inconsistency.

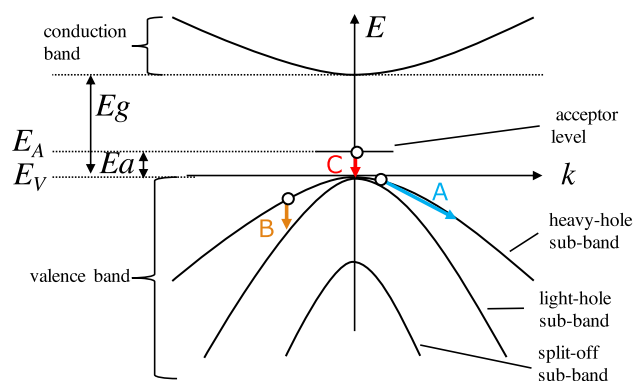


Fig. 3 Schematic view of the band structure of CdZnTe. The horizontal axis shows wave vector k and the vertical one shows energy E . The valence band is separated into three sub-bands: the heavy-hole, light-hole, and split-off sub-bands. The energy levels of the top valence band and the acceptor are denoted by E_V and E_A , respectively. The band gap energy is denoted by E_g and the gap energy between acceptor level and the valence band is E_a . The transitions A, B, and C are the absorption transitions of the model described in the text.

Discussion

In this section, we discuss absorption causes in CdZnTe. As shown in the previous section, our result reveals that α increases at the cryogenic temperature, contrary to the free-carrier expectation. This disparity suggests that, in addition to free-carrier absorption, other causes influence the absorption coefficient.

Absorption Model

To discuss the dominant absorption cause, we built a model of the α of CdZnTe. To discuss the causes at room temperature, we included the absorption causes considered in the CdZnTe study at room temperature⁵ in our model. Figure 3 shows a schematic view of the band structure of p -type CdZnTe and hole transitions related to absorption in the model. At room temperature, p -type CdZnTe absorbs due to two types of free-carrier transition: (A) transitions within the same valence sub-band, (B) transitions from the heavy-hole sub-band to the light-hole sub-band, as in e.g.¹⁷ According to the room-temperature study, CdZnTe has attenuation due to Te precipitates and the lattice absorption.⁵

The absorption causes in CdZnTe are well discussed at room temperature,⁵ but they are not studied at low temperatures. As a result, we include the absorption causes considered in a previous cryogenic CdTe study¹⁸ to discuss the temperature dependence of the absorption coefficient. In this case, we assume that the physical properties of CdZnTe are

similar to those of CdTe due to the low Zn abundance ratio (~ 4%). Čápek et al.¹⁸ showed the existence of absorption of the hole transition from the acceptor level to the valence band (C in Fig. 3).

The total absorption coefficient α_{model} is expressed as

$$\alpha_{\text{model}} = N_{\text{free}}(\sigma_{\text{intra}} + \sigma_{\text{inter}}) + N_{\text{trapped}}\sigma_{\text{trapped}} + \alpha_{\text{Te}} + \alpha_{\text{lattice}}, \tag{6}$$

where σ_{intra} , σ_{inter} , and σ_{trapped} are the absorption cross-sections of the (A) intraband, (B) interband, and (C) acceptor-valence band transition, respectively. The density of free holes is denoted by N_{free} , while the density of trapped holes is denoted by N_{trapped} . Attenuation due to Te precipitates is denoted by α_{Te} , and the lattice absorption is denoted by α_{lattice} .

The Drude model, as in e.g.,¹⁹ is used to calculate the cross-section of (A) intraband absorption σ_{intra} . The absorption coefficient in the Drude model can be calculated using the equation of motion of a free carrier with an attenuation term. We derive the σ_{intra} as

$$\begin{aligned} \sigma_{\text{intra}} &= \frac{q^2}{\pi n c^5 m^* \tau_R(T) \tilde{\nu}^2} \\ &= b_0 \left(\frac{\tilde{\nu}}{943 \text{ cm}^{-1}} \right)^{-2} \left(\frac{T}{300 \text{ K}} \right)^{-1.5}, \end{aligned} \tag{7}$$

where b_0 is a proportional factor, $\tilde{\nu}$ is the wavenumber ($\tilde{\nu} = 1/\lambda$), q is the effective charge, n is the refractive index, c is the light speed, m^* is the effective mass, and τ_R is the relaxation time. The relaxation time τ_R is the mean time interval of free-hole collisions with main scatterers. We assume that τ_R is proportional to $T^{-1.5}$ because lattice vibrations at $T = 100\text{-}300$ K primarily caused the carrier scattering for CdTe case.¹⁶ Although the temperature dependence of hole mobility is not proportional to $T^{-1.5}$ at $T < 100$ K, we assume that at such low temperatures intraband absorption becomes negligible because of free-hole freeze-out. Therefore, we apply the single power-law function as the $\tau_R(T)$ in the model.

Next, we describe the cross-section of (B) interband absorption σ_{inter} . We consider the absorption cross-section of the direct transition of holes from the heavy-hole sub-band to the light-hole sub-band. In this case, we assume that the bands have spherical energy surfaces with a parabolic dispersion relation and that the occupational probability at each band has a Maxwellian energy distribution. The cross-section σ_{inter} is estimated in a similar approach as general p-type semiconductors described in Basu¹⁷ as follows:

$$\begin{aligned} \sigma_{\text{inter}} &= a_0 \left(\frac{\tilde{\nu}}{943 \text{ cm}^{-1}} \right)^{0.5} \left(\frac{T}{300 \text{ K}} \right)^{-1.5} \\ &\quad \times \left[1 - \exp \left(-\frac{hc\tilde{\nu}}{k_B T} \right) \right] \exp \left(-a_1 \frac{hc\tilde{\nu}}{k_B T} \right), \end{aligned} \tag{8}$$

$$a_1 = \left(\frac{m_h}{m_l} - 1 \right)^{-1}, \tag{9}$$

where a_0 is a proportional factor, m_h/m_l is the effective mass ratio of heavy and light holes and h is the Planck constant.

We discuss the cross-section of (C) trapped-hole absorption σ_{trapped} . Čápek et al.¹⁸ measured the α of CdTe at cryogenic temperature and concluded that the trapped-hole absorption exists. We assume that the cross-section σ_{trapped} is a function of wavelength but not of temperature. This assumption is made because the temperature dependence of the absorption cross-section is primarily due to the temperature dependence of the occupational probability difference between initial acceptor state- i and final state- j in the valence band ($f_i - f_j$).¹⁷ At low temperatures in the acceptor state, the majority of the holes will be trapped, and free holes will be exhausted. Because trapped-hole absorption will be dominant at cryogenic temperatures, we assume that $f_i \sim 1, f_j \sim 0$ and trapped-hole cross-section is temperature independent.

We then describe the densities of free holes N_{free} and trapped holes N_{trapped} . There are two possible types of free holes. One is ‘‘intrinsic’’ free holes, which are released by the transition from the conduction band to the valence band, and the other is ‘‘extrinsic’’ free holes, which are released by the transition from an acceptor band to the valence band. The total free-hole density at the room temperature can be estimated with the resistivity $\rho = 50\text{-}130 \text{ }\Omega\text{cm}$ as

$$N_{\text{free}}(300 \text{ K}) = \frac{1}{q\rho\mu} = (9 \pm 5) \times 10^{14} \text{ cm}^{-3}, \tag{10}$$

where q is the charge of a single hole. We assume that the hole mobility μ is the same as that of CdTe ($\mu = 80 \text{ cm}^2\text{V}^{-1}\text{sec}^{-1}$,¹⁶) because of the low percentage of Zn (~ 4%) in our CdZnTe samples. On the other hand, the intrinsic hole density at room temperature is estimated as

$$\begin{aligned} N_{\text{free,intrinsic}}(300 \text{ K}) &= 2 \left(\frac{k_B T}{2\pi\hbar^2} \right)^{3/2} (m_{e^*} m_h^*)^{3/4} \exp \left(-\frac{E_g}{2k_B T} \right) \\ &\sim 10^6 \text{ cm}^{-3}, \end{aligned} \tag{11}$$

where m_h^* is the effective hole mass ($m_h^*/m_e = 0.30$ for CdTe),²⁰ m_{e^*} is the effective electron mass ($m_{e^*}/m_e = 0.11$ for CdTe),²⁰ and E_g is the band gap energy between the valence band and the conduction band ($E_g \sim 1.5 \text{ eV}$).^{3,15} The free holes at room temperature are dominated by the extrinsic free holes released from the acceptor level, and we ignore the intrinsic free holes. At lower temperatures, the ratio of the extrinsic-free-hole density to the intrinsic-free-hole density becomes larger since the intrinsic energy gap is larger than that between the acceptor band and the valence band. Therefore, we also ignore the intrinsic free holes at lower temperatures.

We derive the temperature dependence of the N_{free} similarly to that of Ahmad.¹⁶ We obtain an analytical equation of the free-hole density by coupling the following three equations: the equation for the density of holes trapped at the acceptor level, the equation for free-hole density based on the effective density of states, and the conservation equation of the sum of the free and trapped-hole densities. We derive the N_{free} as

$$N_{\text{free}} = N_A \frac{2}{\sqrt{1 + 8(N_A/N_V) \exp(E_a/k_B T) + 1}}, \quad (12)$$

where N_A is the acceptor density, N_V is the effective density of states, E_a is the energy gap between the acceptor level and the valence band's top. In this case, we assume that there is a single acceptor level since Ahmad¹⁶ explained the temperature dependence of the CdTe free-hole density measured by them with a single-acceptor-level model. We also assume that the effect of the donor is negligible. In this equation, N_{free} is roughly constant in a relatively high-temperature range (namely saturation regime) due to full ionization of acceptors, in a relatively low-temperature range (namely the ionization regime), whereas N_{free} is proportional to $\exp(-E_a/2k_B T)$.¹⁶ According to Kittel,¹⁵ the effective density of states N_V is given by

$$N_V = 2(2\pi m_* k_B T / h^2)^{3/2} \\ = 4.12 \times 10^{18} \left(\frac{m_*}{0.3m_e} \right)^{3/2} \left(\frac{T}{300 \text{ K}} \right)^{3/2} \text{ cm}^{-3}, \quad (13)$$

where m_* represents the effective hole mass ($m_*/m_e = 0.30$ for CdTe)²⁰. The acceptor is assumed to be fully ionized at $T \sim 300 \text{ K}$ ¹⁶ and the free-carrier density is assumed to be almost the same as the acceptor density. Thus, the acceptor density is estimated as

$$N_A \sim N_{\text{free}}(300 \text{ K}) = (9 \pm 5) \times 10^{14} \text{ cm}^{-3}. \quad (14)$$

In this model, we assume the N_A value as $N_A = 9 \times 10^{14} \text{ cm}^{-3}$. We estimate the uncertainty of N_A as $\pm 5 \times 10^{14} \text{ cm}^{-3}$ from the uncertainty of the room-temperature resistivity. The effect of the uncertainty of N_A is discussed in the next subsection. Because the sum of the free-hole density N_{free} and the trapped-hole density N_{trapped} equals the acceptor density N_A , the trapped-hole density N_{trapped} is expressed as

$$N_{\text{trapped}} = N_A - N_{\text{free}}. \quad (15)$$

We then discuss how the attenuation due to Te precipitates α_{Te} affects our model. Sarugaku et al.⁵ evaluated Mie scattering attenuation due to Te precipitates as $\alpha_{\text{Te}} \leq 0.01 \text{ cm}^{-1}$ at $\lambda > 5 \mu\text{m}$. Subsequently, because Te precipitate size in our samples is limited to $\leq 2 \mu\text{m}$ in the same way in their

samples, we assume that α_{Te} in our samples is as small as $\leq 0.01 \text{ cm}^{-1}$. Also, the scattering attenuation is unaffected by temperature. As a result, we ignore the α_{Te} assuming it makes only a minor small contribution to the α_{model} .

In addition, we discuss the lattice absorption α_{lattice} . Based on the empirical exponential relationship, α_{lattice} at room temperature is less than $2 \times 10^{-3} \text{ cm}^{-1}$ at $\lambda < 15.1 \mu\text{m}$, according to Sarugaku et al.⁵ The lattice absorption strength is proportional to the difference in phonon creation and annihilation probabilities. The strength of a single-phonon process is unaffected by temperature, whereas the strength of a multi-phonon process decreases with temperature.¹⁹ Therefore, α_{lattice} is less than $2 \times 10^{-3} \text{ cm}^{-1}$ at all temperatures and wavelengths measured. Because α_{lattice} is negligible compared to the total absorption coefficient, we ignore it in our model.

To summarize the above discussion, we set our absorption model as follows:

$$\alpha_{\text{model},\nu} = N_{\text{free}}(T)(\sigma_{\text{intra},\nu}(T) + \sigma_{\text{inter},\nu}(T)) \\ + N_{\text{trapped}}(T)\sigma_{\text{trapped}}. \quad (16)$$

The free parameters are the acceptor energy (E_a), the effective mass ratio (m_h/m_l) and three proportional factors (b_0 , a_0 , σ_{trapped}).

Model Fittings and Discussion

This section discusses what causes absorption in CdZnTe by fitting our results with the absorption model described above. Because the wavelength dependence of σ_{trapped} is unknown, we perform fitting individually in each wavelength band. Figure 4 shows the model fitting result in each band ($\lambda = 6.45, 10.6, 11.6, 15.1 \mu\text{m}$). Each fitted parameter is listed in Table III. The N_A value is fixed to $N_A = 9 \times 10^{14} \text{ cm}^{-3}$ as discussed in the previous subsection. It is worth noting that, in the fitting in the $6.45 \mu\text{m}$ band, the b_0 value is fixed to $b_0 = 1 \times 10^{-16} \text{ cm}^2$ based on the best-fit value in the other wavelength bands to secure convergence of the fitting. This is because intraband absorption becomes smaller in the shorter wavelength band due to its wavelength dependence and it is difficult to fit the parameter b_0 at the shortest wavelength $6.45 \mu\text{m}$.

Like the measured results, the model shows an increase in the absorption coefficient at low temperatures and reproduces the measured temperature dependence across the entire temperature range. Two physical parameters (E_a , m_h/m_l) and two proportional factors (a_0 , b_0) are consistent within 1σ uncertainty range among each wavelength band case. This fitting result shows that, in the temperature range of $T = 50\text{--}150 \text{ K}$, the dominant holes change from free holes to trapped holes, and the dominant absorption

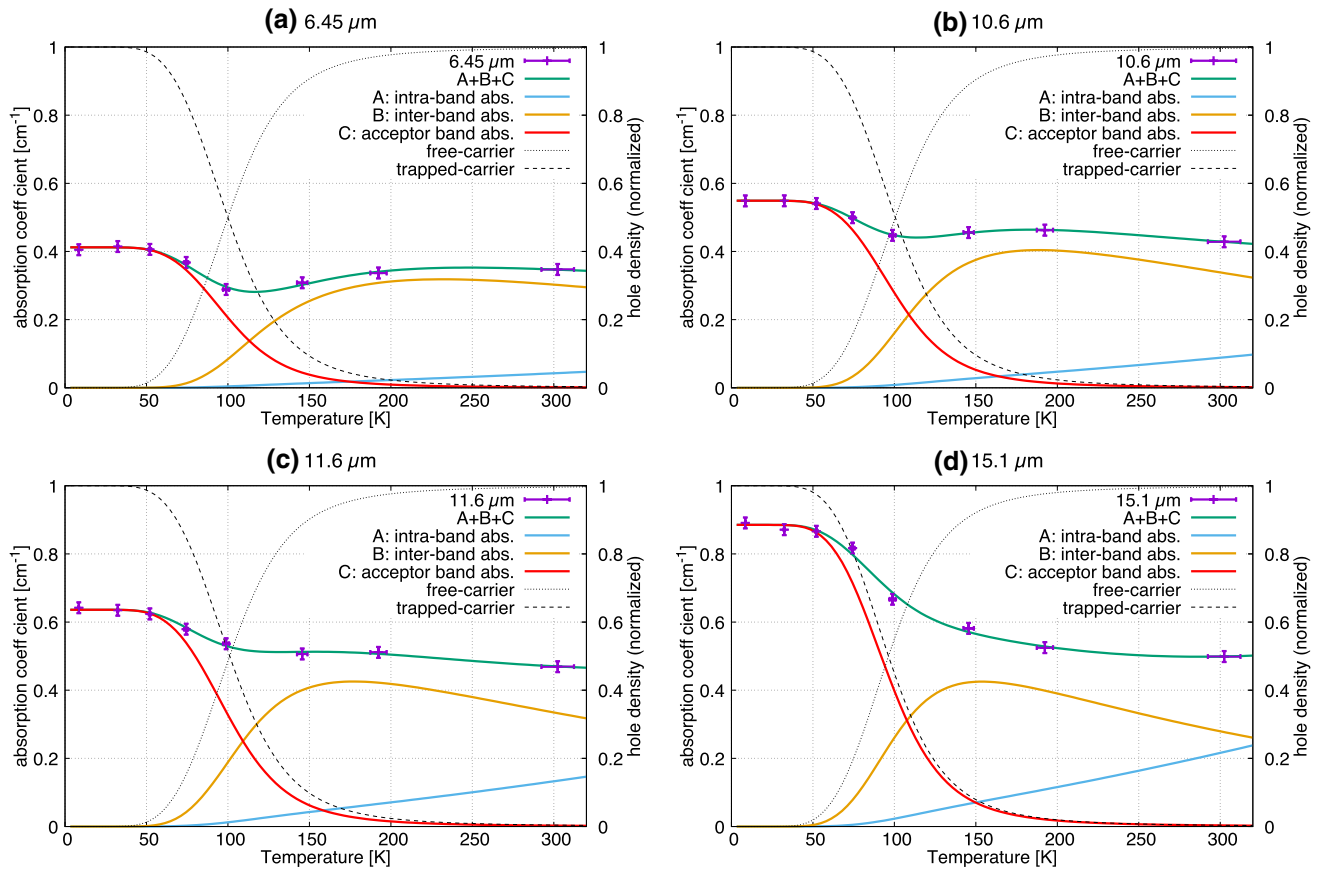


Fig. 4 The temperature dependence of the absorption coefficient of the CdZnTe in the $\lambda =$ **a** 6.45, **b** 10.6, **c** 11.6, and **d** 15.1 μm bands and the fitted model. The purple points show the measured α . The error bars show 1σ uncertainty ranges. Green solid lines show the total fitted absorption model. Sky-blue dashed, orange dotted, and red

dashed-dotted lines show the fitted models of intraband, interband, and acceptor band absorption, respectively. The black dotted and dashed lines show the normalized density of free holes and trapped holes, respectively, by the right scale of the vertical axis (Color figure online).

Table III Parameters fitted at each wavelength band and reference value. The acceptor density N_A is fixed to $N_A = 9 \times 10^{14} \text{ cm}^{-3}$. The errors show 1σ uncertainties. The derivation of the reference values is described in the text. NDF denotes the degrees of freedom

Band	6.45 μm	10.6 μm	11.6 μm	15.1 μm	Reference value
E_a [meV]	59 ± 4	59 ± 4	59 ± 7	59 ± 6	$\sim 60, \sim 58.7^{*b}$
m_h/m_l	7.5 ± 0.5	6.3 ± 0.7	6 ± 1	6 ± 1	$\sim 5, \sim 7^{*c}$
a_0 [10^{-16} cm^2]	9 ± 1	9 ± 2	8 ± 3	8 ± 3	–
b_0 [10^{-16} cm^2]	1 (fixed) ^d	1.0 ± 0.6	1.2 ± 0.7	1.0 ± 0.4	–
σ_{trapped} [10^{-16} cm^2]	4.6 ± 0.1	6.10 ± 0.07	7.1 ± 0.1	9.8 ± 0.1	$5\text{--}13^{*e}$
Reduced- χ^2	0.23	0.008 ^{*f}	0.21	1.3	
NDF	4	3	3	3	

^b The values from past CdTe studies. [16,21](#)

^c The values from past CdTe studies. [18,22](#)

^d The b_0 value is fixed to secure convergence.

^e The predicted value based on the CdTe cryogenic absorption cross-section. [18](#)

^f For the 10.6 μm band case, the reduced- χ^2 is extremely small.

This is probably because the uncertainty $\Delta\alpha$ is overestimated. The uncertainty $\Delta\alpha$ is estimated based on the reproducibility of the measurement at 300 K before and after the cooling cycle. For measurement in the near temperature range, the uncertainty may be smaller than the estimated $\Delta\alpha$ because of the small displacement of the holder caused by a thermal shrink.

causes changes from free holes (A, B) to trapped holes (C) with cooling.

Additionally, we compare derived physical parameters (E_a , m_h/m_l) to the previous studies to see if the fitted-parameter values are consistent with the previous measurements. We compare the best-fit acceptor energy E_a to that of CdTe. The acceptor energy of Na-doped CdTe has been reported to be ~ 60 meV using a Hall effect measurement¹⁶ and ~ 58.7 meV using a photoluminescence measurement.²¹ The best-fitted acceptor energies ($E_a \sim 59$ meV) are consistent at 1σ uncertainty level with previous CdTe studies. Following that, we compare the effective mass ratio m_h/m_l . The best-fitted values of the effective mass ratio ($m_h/m_l = 6-7$) are within the range of reported values by previous CdTe studies ($m_h/m_l \sim 7$,¹⁸ ~ 5).²² These reference values based on previous studies are also listed in Table III. Following the above comparison, the measured absorption coefficients and their temperature dependence are well-fitted with the absorption model by free/trapped holes and reasonable physical parameters (E_a , m_h/m_l).

Moreover, we discuss the validity of the temperature dependence of the best-fit σ_{trapped} . In this study, we assume that the trapped-hole cross-section σ_{trapped} is temperature independent as mentioned in the previous subsection. At $T < 50$ K, the best-fit results show that the trapped-hole absorption is dominant. We conclude that the assumption of independence is reasonable, owing to the inability to see the temperature dependence of the α at < 50 K.

To validate the σ_{trapped} values, we compare the best-fit σ_{trapped} with a previous CdTe study, which is a similar substance used in the current study. Čápek et al.¹⁸ measured the α of p -type CdTe with $N_{\text{free}}(300\text{K}) = 3.1 \times 10^{17} \text{ cm}^{-3}$ free-hole density. We assume that the trapped-hole density at 80 K is the same as the $N_{\text{free}}(300 \text{ K})$ because the free-carrier density of CdTe and CdZnTe decreases with cooling¹⁶ as well as that of CdZnTe. As a result, the CdTe cross-section $\sigma_{\text{trapped,CdTe}}$ can be estimated as follows:

$$\sigma_{\text{trapped,CdTe}} = \alpha(80 \text{ K})/N_{\text{trapped}}(80 \text{ K}) = \alpha(80 \text{ K})/N_{\text{free}}(300 \text{ K}). \quad (17)$$

CdTe α values are taken from Fig. 3 of Čápek et al.¹⁸ The $\sigma_{\text{trapped,CdTe}}$ is calculated as $(5, 9, 10, 13) \times 10^{-16} \text{ cm}^2$ at $\lambda = 6.45, 10.6, 11.6, \text{ and } 15.1 \mu\text{m}$, respectively. As a reference, the cross-sections σ_{trapped} derived for CdTe are also listed in Table III. Also, because the best-fit σ_{trapped} in the current study is of the same order of magnitude as the $\sigma_{\text{trapped,CdTe}}$, we conclude that the best-fit CdZnTe cross-section σ_{trapped} is within a reasonable range when compared to that derived for CdTe.

In addition, we estimate the effect of the uncertainty of the acceptor density value N_A . Based on Eq. 12, the acceptor

Table IV The best-fit result in the case of $N_A = (4, 9, 14) \times 10^{14} \text{ cm}^{-3}$. The nominal N_A value is $N_A = 9 \times 10^{14} \text{ cm}^{-3}$

	Case 1	Case 2 (nominal)	Case 3
$N_A [10^{14} \text{ cm}^{-3}]$ (fixed)	4	9	14
E_a [meV]	63 ± 5	59 ± 4	56 ± 4
m_h/m_l	6.5 ± 0.7	6.3 ± 0.7	6.2 ± 0.7
$a_0 [10^{-16} \text{ cm}^2]$	19 ± 4	9 ± 2	6 ± 2
$b_0 [10^{-16} \text{ cm}^2]$	2.5 ± 1	1.0 ± 0.6	0.6 ± 0.4
$\sigma_{\text{trapped}} [10^{-16} \text{ cm}^2]$	13.7 ± 0.2	6.10 ± 0.07	3.92 ± 0.05

density is assumed to be $N_A = 9 \times 10^{14} \text{ cm}^{-3}$ as discussed in the previous subsection. From the uncertainty of the room-temperature resistivity, the uncertainty of the acceptor density is estimated as $\pm 5 \times 10^{14} \text{ cm}^{-3}$. To estimate the effect of the uncertainty of the acceptor density, we perform the parameter fitting in the $10.6 \mu\text{m}$ band in the cases of $N_A = 4 \times 10^{14}, 14 \times 10^{14} \text{ cm}^{-3}$. The fitting result is listed in Table IV. As shown in Table IV, the best-fit E_a values are ~ 60 meV and the best-fit m_h/m_l values are ~ 6 for all the N_A cases. The best-fit σ_{trapped} values are of the same order of magnitude as that derived for CdTe above ($\sim 9 \times 10^{-16} \text{ cm}^2$). We conclude that the uncertainty of the N_A has a minor effect on the estimation of the E_a and m_h/m_l but affects the best-fit value of $a_0, b_0, \sigma_{\text{trapped}}$ by a factor.

In summary, the absorption coefficient due to free holes decreases and becomes negligible at $T < 50$ K, just as we initially predicted.⁵ However, this is insufficient to explain the temperature dependence of the measured absorption coefficient. At cryogenic temperatures, the absorption coefficient due to trapped holes increases and becomes dominant at $T < 50$ K. Čápek et al.¹⁸ showed the existence of the trapped-hole absorption in CdTe. Our study reveals that the trapped-hole absorption is observed also in CdZnTe. We note that Čápek et al.¹⁸ did not show the temperature dependence of the absorption by physical models, while our study reveals that the temperature dependence of the absorption coefficient is explained with the model from room temperature to low temperatures.

Moreover, we can predict the cryogenic absorption coefficient from the room-temperature resistivity based on the absorption model. According to the model, the cryogenic absorption is primarily caused by carriers trapped at the impurity level. The cryogenic trapped-carrier density is roughly the same as the free-carrier density at room temperature because carriers trapped in the acceptor level at $T < 50$ K are released to the valence band at $T \sim 300$ K. Also, the free-carrier density is known to be inversely proportional to the resistivity ρ . Hence, considering the above

Table V Properties of the high-resistivity CdZnTe single crystals

Sample	Incident-surface size [mm ²]	Thickness [mm]	Resistivity [Ωcm]	Conductivity type	Te particle size [μm]	Ra [nm]
HighR-t1	10 × 10	0.79	$> 10^{10}$	<i>n</i>	< 2	< 1
HighR-t10	7 × 7	9.94	$> 10^{10}$	<i>n</i>	< 2	< 1

relationships, we derive an equation connecting cryogenic ($T < 50$ K) trapped-carrier absorption and the room-temperature resistivity as follows:

$$\begin{aligned} \alpha_{\text{trapped}}(T < 50 \text{ K}) &= \sigma_{\text{trapped}} N_{\text{trapped}}(T < 50 \text{ K}) \\ &\simeq \sigma_{\text{trapped}} N_{\text{free}}(T = 300 \text{ K}) \propto 1/\rho(T = 300 \text{ K}). \end{aligned} \quad (18)$$

While trapped carriers play a dominant role in absorbance, we can predict the cryogenic absorption coefficient from the room-temperature resistivity using the inversely proportional relation.

Furthermore, we discuss the requirement of resistivity for application to a mid-infrared cryogenic immersion grating. The requirement of absorption coefficient of the immersion grating is $\alpha < 0.01 \text{ cm}^{-1}$.¹⁴ Based on Eq. 18 and our measurement results, to meet the α requirement, CdZnTe must have $\rho(T = 300 \text{ K}) > 10^4 \Omega\text{cm}$. We also measure the α value of a high-resistivity CdZnTe in Appendix A to see if it meets the α requirement. The high-resistivity CdZnTe results are consistent with the prediction based on the room-temperature resistivity (see Appendix A).

In addition, we anticipate that we can apply this model to other semiconductors to evaluate the cryogenic absorption coefficient (e.g., other semiconductor-type immersion gratings). This is because absorption causes in the model are common in general semiconductors,¹⁷ and are not unique to CdZnTe.

Conclusions

We measured the transmittance of CdZnTe substrates with two different thicknesses and estimated the absorption coefficient α in the $\lambda = 6.45, 10.6, 11.6,$ and $15.1 \mu\text{m}$ bands at $T = 8.6\text{--}300 \text{ K}$. At $T \sim 300 \text{ K}$, the estimated α range is $\alpha = 0.3\text{--}0.5 \text{ cm}^{-1}$ which increases to $\alpha = 0.4\text{--}0.9 \text{ cm}^{-1}$ at cryogenic temperatures ($T = 8.6 \pm 0.1 \text{ K}$). Based on the physical absorption model, we propose that the dominant absorption cause at $T = 150\text{--}300 \text{ K}$ is attributed to free holes: the dominant absorption cause at cryogenic temperature is attributed to trapped holes. Moreover, we discuss a method to predict the CdZnTe absorption coefficient at cryogenic temperature based on the room-temperature resistivity.

Appendix A: Absorption Coefficient of the High-Resistivity CdZnTe

As discussed in the main text, the absorption coefficient of a higher-resistivity CdZnTe is lower than that of a low-resistivity CdZnTe. We measure the absorption coefficient of a high-resistivity-type CdZnTe to see if it has low absorption at cryogenic temperatures.

First, we describe the high-resistivity CdZnTe sample and the measurement method. As listed in Table V, the samples in this appendix are *n*-type high-resistivity ($\rho > 10^{10} \Omega\text{cm}$) CdZnTe substrates, while those in the main text are *p*-type low-resistivity ($\rho \sim 10^2 \Omega\text{cm}$) CdZnTe substrates. We prepare thin and thick samples, highR-t1 and highR-t10. The other conditions (surface roughness, Te-precipitate size, manufacturer) are the same as those described in the main text for samples. It is worth noting that highR-t1 and highR-t10 are cut from different ingots. However, because they are manufactured in the same way, we assume that their absorption coefficients and reflectivity are similar. The measurement method is the same as that described in the main text.

Next, we describe the measurement result of the high-resistivity CdZnTe. Figure 5 shows the α of the high-resistivity CdZnTe at each temperature and wavelength. Also, because all the measured α are neither significantly above nor below zero, we set the 5σ upper limits of the $\alpha < 0.11 \text{ cm}^{-1}$. α of the high-resistivity CdZnTe is lower than that of the low-resistivity one ($\alpha > 0.35 \text{ cm}^{-1}$) in the main text at all the measured wavelengths and temperatures.

Following that, we compare our result with the previous result at room temperature. Kaji et al.¹³ revealed that CdZnTe with lower resistivity absorbed more at room temperature. The room-temperature α of the CdZnTe with a resistivity of $\rho = 3.5 \times 10^{10} \Omega\text{cm}$ measured by them is less than 0.01 cm^{-1} in the wavelength range of $\lambda = 6.45\text{--}15.1 \mu\text{m}$. The room-temperature absorption coefficient measured by them and that measured by us are consistent, although we can only restrict α 's upper limit. In addition, our result reveals that CdZnTe with lower resistivity has higher absorption even in the temperature range of $8.6\text{--}300 \text{ K}$, whereas they revealed this relation only at room temperature ($T \sim 295 \text{ K}$).

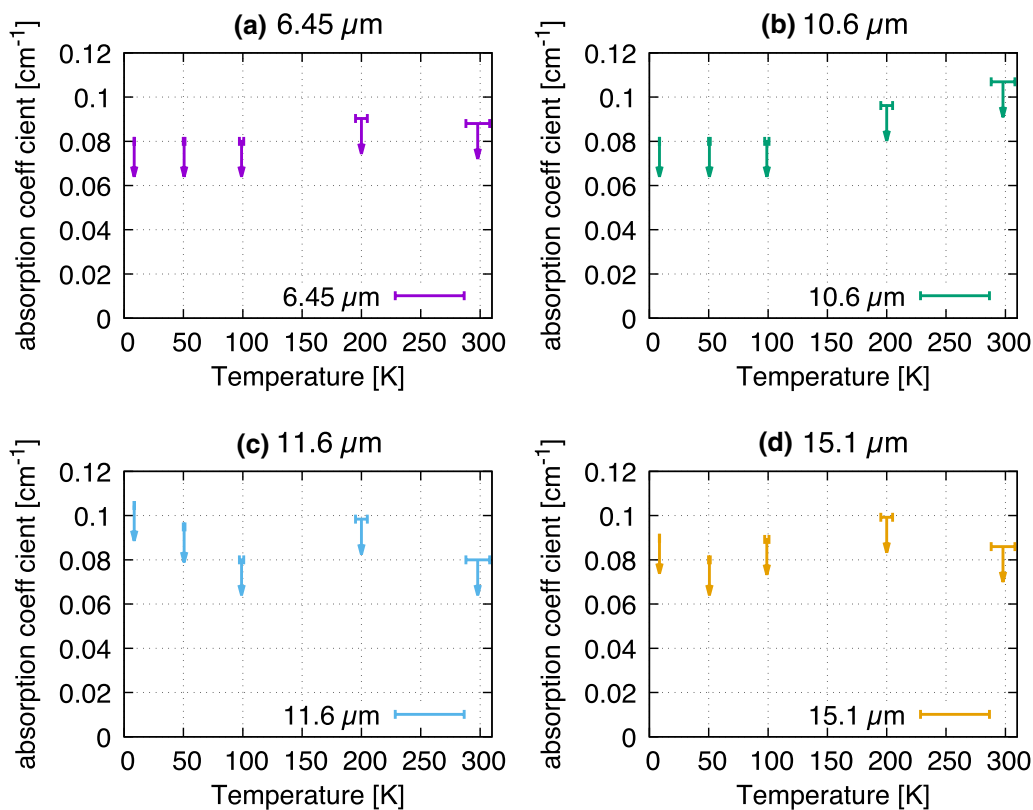


Fig. 5 The upper limits of the α of the high-resistivity CdZnTe in the **a** 6.45, **b** 10.6, **c** 11.6, and **d** 15.1 μm bands. Purple, green, sky-blue, and orange arrows show the 5σ upper limit of the α in the 6.45, 10.6, 11.6, and 15.1 μm bands, respectively (Color figure online).

Next, we compare the high-resistivity CdZnTe with the α prediction based on room-temperature resistivity. As discussed in the main text, the trapped-carrier absorption coefficient is inversely proportional to resistivity and mobility. According to the model, the main absorption cause is trapped-carrier absorption. Because the low-resistivity CdZnTe is *p*-type and the high-resistivity CdZnTe is *n*-type, we consider the absorption due to electrons trapped at the donor level. We assume that electron mobility is the same as in CdTe ($\sim 700 \text{ cm}^2\text{V}^{-1}\text{sec}^{-1}$, ²⁰). We also assume that trapped electron absorption follows the same order as trapped-hole absorption. Under these assumptions, the estimated absorption coefficient due to trapped electrons is negligible ($\alpha < 10^{-9} \text{ cm}^{-1}$). As a result, we consider the lattice absorption α_{lattice} and Te-precipitates attenuation α_{Te} , as dominant causes, which are ignored in the main text. As discussed in the main text, the sum of α_{lattice} and α_{Te} at $T=8.6 \text{ K}$ is considered to be less than that at $T = 300 \text{ K}$ ($\alpha < 0.006 \text{ cm}^{-1}$ at $\lambda = 6.45\text{--}15.1 \mu\text{m}$). Therefore, we can predict that the α of the high-resistivity CdZnTe at 8.6 K is $\alpha < 0.006 \text{ cm}^{-1}$. Our result is consistent with this prediction, although α has such a large uncertainty that we can only obtain the upper limit of the α . A more precise measurement system is needed to reveal the temperature dependence of

the α of high-resistivity CdZnTe because the α is lower than the uncertainty of our measurement system.

Appendix B: Sample holders

Figure 6 shows the sample holders for thick and thin samples. To secure thermal contact, we screw the top of the thick-sample holders to the cold head surface with screws and hold them from the side with a copper plate and indium sheets. To monitor the temperature of the sample, we place a calibrated Cernox temperature sensor (CX-1030-SD-HT-1.4L; Lakeshore inc.) on the side of the sample. A temperature monitor (Model 218, Lakeshore inc.) is used to monitor the sensor signal. On the other hand, the thin sample is clamped between the thin-sample holder and the holding plate. We screw the thin-sample holder to the cold head and insert indium sheets between the sample and the thin-sample holder to secure thermal contact. To monitor the sample temperature, we use the same temperature sensor used in the thick-sample case on the holder.

Acknowledgments We thank Mr. A. Noda and Dr. R. Hirano of JX Nippon Mining & Metals Corporation for valuable comments. We

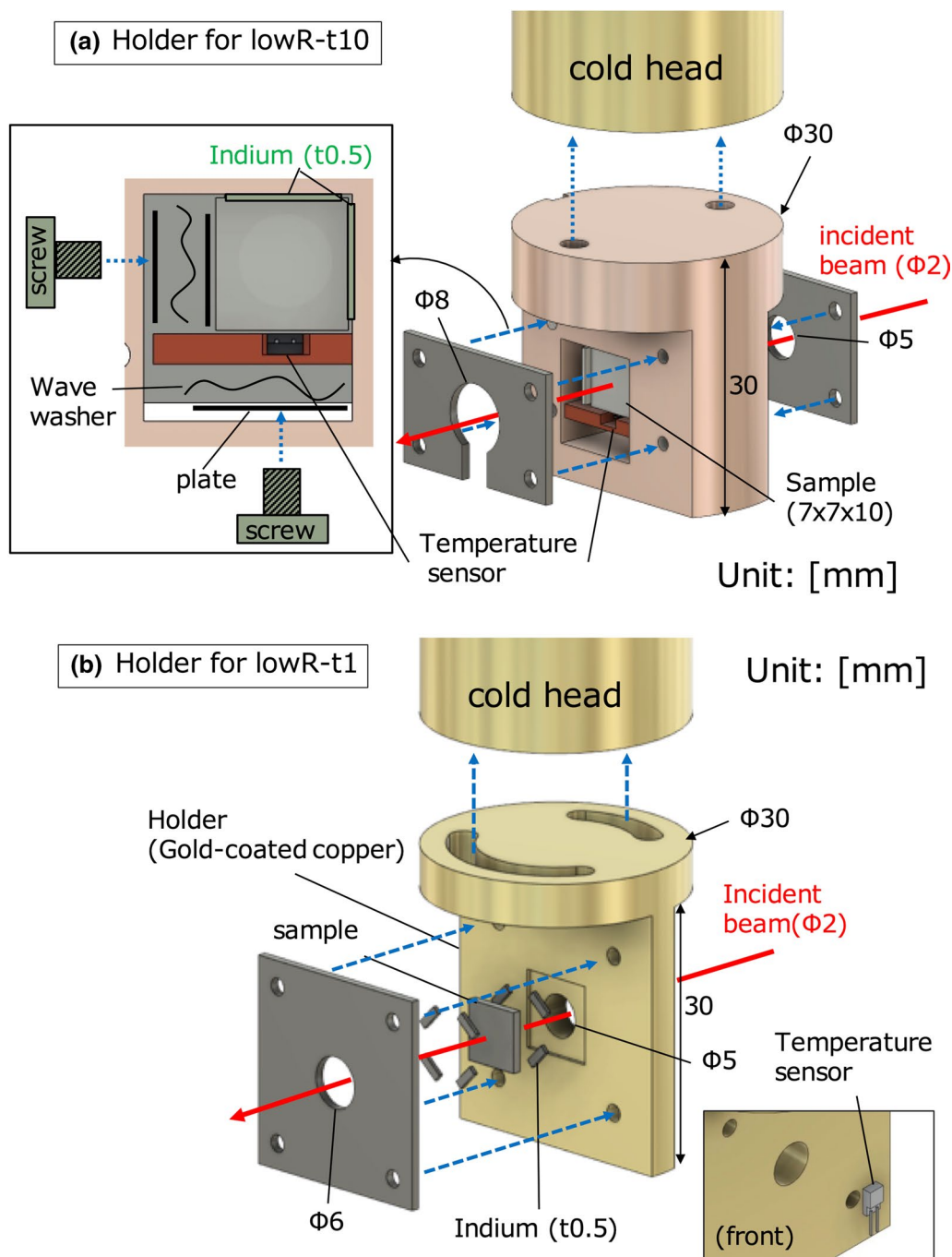


Fig. 6 Two types of sample holder: **a** holder for the lowR-t10 sample and **b** holder for the lowR-t1 sample. Holders are screwed to the cold head of the cryostat. Red arrows show the beam path. Blue dashed

arrows indicate screwed-in points. Dimensions are in millimeters. Details are described in the text (Color figure online).

appreciate members of the Laboratory of Infrared High-resolution Spectroscopy (LIH) at Kyoto Sangyo University for informative advice on immersion grating and experiments for its material selections. This research is part of conceptual design activity for the infrared astronomical space mission SPICA, which was a candidate for the ESA Cosmic Vision M5 and JAXA strategic L-class mission. We appreciate the production of the holders and technical support by the Instrument Development Center in Nagoya University. We are grateful for the

technical assistance to construct the measurement system by Mr. R. Ito. We appreciate Dr. J. Kwon and Mr. R. Doi for their supports in preliminary experiments prior to this study. H.M. is supported by the Advanced Leading Graduate Course for Photon Science (ALPS) of the University of Tokyo.

Conflict of interest The authors declare that they have no conflict of interest.

Open Access This article is licensed under a Creative Commons Attribution 4.0 International License, which permits use, sharing, adaptation, distribution and reproduction in any medium or format, as long as you give appropriate credit to the original author(s) and the source, provide a link to the Creative Commons licence, and indicate if changes were made. The images or other third party material in this article are included in the article's Creative Commons licence, unless indicated otherwise in a credit line to the material. If material is not included in the article's Creative Commons licence and your intended use is not permitted by statutory regulation or exceeds the permitted use, you will need to obtain permission directly from the copyright holder. To view a copy of this licence, visit <http://creativecommons.org/licenses/by/4.0/>.

References

1. Y. Eisen and A. Shor, CdTe and CdZnTe materials for room-temperature X-ray and gamma ray detectors. *J. Cryst. Growth* 184–185, 1302 (1998).
2. P. Norton, HgCdTe infrared detectors. *Opto-Electron. Rev.* 10, 159 (2002).
3. A. Noda, H. Kurita, and R. Hirano, in *Mercury Cadmium Telluride: Growth, Properties and Applications*. ed. by P. Capper, J. Garland (Wiley, West Sussex, 2011), p. 21.
4. T.F. Deutsch, Laser window materials-an overview. *J. Electron. Mater.* 4, 663 (1975).
5. Y. Sarugaku, S. Kaji, Y. Ikeda, N. Kobayashi, T. Sukegawa, T. Nakagawa, H. Kataza, S. Kondo, C. Yasui, K. Nakanishi, and H. Kawakita, Infrared attenuation spectrum of bulk high-resistivity CdZnTe single crystal in transparent wavelength region between electronic and lattice absorptions. *J. Electron. Mater.* 46, 282 (2017).
6. T. Wada, H. Kaneda, T. Kokusho, T. Suzuki, K. Morihana, T. Tsuchikawa, Y. Kuroda, D. Ishikawa, S. Oyabu, N. Isobe, D. Ishihara, H. Matsuhara, K. Nagase, T. Nakagawa, T. Ootsubo, M. Yamagishi, H. Maeshima, S. Onishi, K. Matsumoto, S. Itoh, M. Uchiyama, R. Lau, H. Ebihara, H. Inami, K. Kawabata, Y. Kasaba, T. Sakanoi, Y. Ita, M. Akiyama, I. Sakon, T. Kamizuka, T. Miyata, K. Tsumura, M. Naruse, Y. Ohyama, S.y. Wang, and H. Shibai, in *Proc. SPIE* (2020), p. 114436G.
7. T. Nakagawa, K. Goto, H. Kaneda, H. Matsuhara, J. Matsumoto, T. Mizutani, H. Ogawa, M. Saijo, Y. Sato, K. Sawada, H. Shibai, K. Shinozaki, H. Sugita, S. Takeuchi, C. Tokoku, T. Tirolien, and H. Uchida, in *Proc. SPIE* (2020), p. 1144328.
8. ...P.R. Roelfsema, H. Shibai, L. Armus, D. Arrazola, M. Audard, M.D. Audley, C.M. Bradford, I. Charles, P. Dieleman, Y. Doi, L. Duband, M. Eggens, J. Evers, I. Funaki, J.R. Gao, M. Giard, A. Di Giorgio, L.M. Fernández, M. Griffin, F.P. Helmich, R. Hijmering, R. Huisman, D. Ishihara, N. Isobe, B. Jackson, H. Jacobs, W. Jellema, I. Kamp, H. Kaneda, M. Kawada, F. Kemper, F. Kerschbaum, P. Khosropanah, K. Kohno, P.P. Kooijman, O. Krause, J. Van Der Kuur, J. Kwon, W.M. Laauwen, G. De Lange, B. Larsson, D. Van Loon, S.C. Madden, H. Matsuhara, F. Najarro, T. Nakagawa, D. Naylor, H. Ogawa, T. Onaka, S. Oyabu, A. Poglitsch, V. Reveret, L. Rodriguez, L. Spinoglio, I. Sakon, Y. Sato, K. Shinozaki, R. Shipman, H. Sugita, T. Suzuki, F.F. Van Der Tak, J.T. Redondo, T. Wada, S.Y. Wang, C.K. Wafelbakker, H. Van Weers, S. Withington, B. Vandenbussche, T. Yamada, and I. Yamamura, SPICA-a large cryogenic infrared space telescope: unveiling the obscured universe. *Publ. Astron. Soc. Aust.* (2018). <https://doi.org/10.1017/pasa.2018.15>.
9. Y. Ikeda, N. Kobayashi, Y. Sarugaku, T. Sukegawa, S. Sugiyama, S. Kaji, K. Nakanishi, S. Kondo, C. Yasui, H. Kataza, T. Nakagawa, and H. Kawakita, Machined immersion grating with theoretically predicted diffraction efficiency. *Appl. Opt.* 54, 5193 (2015).
10. A. Leitner, The life and work of Joseph Fraunhofer (1787–1826). *Am. J. Phys.* 43, 59 (1975).
11. J.P. Marsh, D.J. Mar, and D.T. Jaffe, Production and evaluation of silicon immersion gratings for infrared astronomy. *Appl. Opt.* 46, 3400 (2007).
12. T. Sukegawa, S. Sugiyama, T. Kitamura, Y. Okura, and M. Koyama, in *Proc. SPIE* (2012), p. 84502V.
13. S. Kaji, Y. Sarugaku, Y. Ikeda, N. Kobayashi, K. Nakanishi, S. Kondo, C. Yasui, and H. Kawakita, in *Proc. SPIE* (2014), p. 914738.
14. Y. Sarugaku, Y. Ikeda, N. Kobayashi, T. Sukegawa, S. Sugiyama, K. Enya, H. Kataza, H. Matsuhara, T. Nakagawa, H. Kawakita, S. Kondo, Y. Hirahara, and C. Yasui, in *Proc. SPIE* (2012), p. 844257.
15. C. Kittel, *Introduction to Solid State Physics*, 8th edn. (Wiley, New York, 1976).
16. F.R. Ahmad, Temperature dependent van der Pauw-Hall measurements on sodium doped single crystalline cadmium telluride. *J. Appl. Phys.* 117, 115701 (2015).
17. P. Basu, *Theory of Optical Processes in Semiconductors: Bulk and Microstructures* (Oxford University Press, Oxford, 2003), p. 583.
18. V. Čápek, K. Zimmerman, Č. Koňák, M. Popova, and P. Polivka, Valence band structure of CdTe. *Phys. Stat. Sol. (b)* 56, 739 (1973).
19. K. Kudo, *Hikari Bussei Kiso [Basics of Optical Physics]* (Ohmsha, Tokyo, 1996).
20. M. Wakaki, S. Takeshita, and K. Eikei, *Physical Properties and Data of Optical Materials*, 1st edn. (CRC Press, Florida, 2007), p. 82.
21. E. Molva, J. Pautrat, K. Saminadayar, G. Milchberg, and N. Magnea, Acceptor states in CdTe and comparison with ZnTe. *General Trends. Phys. Rev. B* 30, 3344 (1984).
22. U. Becker, H. Zimmermann, P. Rudolph, and R. Boyn, Infrared absorption behavior in CdZnTe substrates. *Phys. Stat. Sol. (a)* 112, 569 (1989).

Publisher's Note Springer Nature remains neutral with regard to jurisdictional claims in published maps and institutional affiliations.